Fluctuation and Noise Letters
(2026) 2640007 (14 pages)

DOI: 10.1142/S0219477526400079

Noise Analysis in Screen-Printed Carbon-Black Resistive Gauges Towards Strain Sensors

Quentin Eynaud *, Eléonore Masarweh †, Valeriya Kilchytska ‡,
Nicolas Marchal §, Denis Flandre ¶ and Léopold Van Brandt ‖

ICTEAM, UCLouvain, Place du Levant, 3
Louvain-la-Neuve, 1348, Belgium
**quentin.eynaud@uclouvain.be*
†eleonore.masarweh@uclouvain.be
‡valeriya.kilchytska@uclouvain.be
§nicolas.marchal@uclouvain.be
¶denis.flandre@uclouvain.be
‖leopold.vanbrandt@uclouvain.be

Received 28 April 2025
Revised 11 December 2025
Accepted 9 March 2026
Published 30 April 2026

Communicated by Carmine Ciofi

We investigate the noise performance of screen-printed carbon-black elastoresistors. Our work focuses on the quality of the printed resistors as devices. The noise power spectral density (PSD) is measured for seven target bias currents on fifteen resistors obtained from printing at three different speeds, each providing a set of five resistors with different lengths and hence resistances. The process variations resulting from the different printing speeds ensure a large sample diversity, with inhomogeneities inherent to printed polymer material. The contributions of thermal noise and low-frequency ($1/f$) noise have been extracted separately. The physical origin of the $1/f$ noise is discussed based on previously published models for carbon resistors. The trends of the $1/f$ noise intensity against sample properties are consistent with former works and hence exclude abnormal process-induced material inhomogeneities and defect distributions. We assess the impact of the printed ink resistance and bias current on the total noise power for the three different printing speeds. We finally highlight that signal-to-noise ratios (SNRs) over 100 dB can be achieved for these elastoresistors in practical conditions with interesting trade-offs regarding size and power consumption.

Keywords: Screen-printing; strain sensors; carbon ink; low-frequency noise; $1/f$ noise.

1. Introduction

Polymer thick-film (PTF) resistors and especially carbon-based screen-printed gauges are interesting transducer choices [1–3] for a wide range of applications, e.g.,

*Corresponding author.

strain [1, 2], thermal [2] or even gas [3] sensing, in a wide range of application fields, from structural monitoring of vehicles, aircrafts or civil structures [1, 4–6] to flexible electronics for wearable or even implantable devices contributing to health care [7–11]. Carbon-based PTF can also be found as passive components in flexible power electronics [12, 13] or surge protection in telecommunication circuits [14].

Combining screen-printing inks to tune specific material properties is common practice to enhance specific material properties [1]. Therefore, the resistors in this work are printed with a blend of Micromax™7082M and Micromax™3571 in a 60/40 weight ratio. Resistors printed with Micromax™7082M, a carbon-black-based resistive polymer ink, can be found in several applications, including elastoresistive components [1, 6], fully printed high-gain amplifier, digital-to-analog converter (DAC) and radio-frequency identification (RFID) tags [15, 16], RF absorber [17] or even smart drug blister [7, 9]. On the other hand, the dielectric polymer ink Micromax™3571 is mainly used in blends as an optically tunable dielectric in filter antenna applications [18–20]. The blend of the two chosen inks has been characterized mechanically in [21], with a Young's modulus of 6 to 8 GPa and low residual stresses. Combined with its high resistivity and a gauge factor (GF) expected to range similarly to other carbon-based inks, it makes a good candidate for flexible MEMS applications. Highly-resistive screen-printed carbon-black strain gauges have been reported with a GF of 8.8 for an 8.1 mm long, 340 μm wide and 18 μm thick 875 kΩ resistor, developing a $\Delta R/R$ around 2.76% at 4000 μ strain [1].

Screen-printable carbon-based PTF resistors appear as a low-cost process alternative to etched copper circuitry, price- and energy-wise at once, as waste is reduced and materials are cured instead of fired at high temperatures [22, 23]. Some noise data of commercial carbon-based resistors have become available (cf. Fig. 12-3 in [24]) but their noise performance has been investigated to a lesser extent than conventional strain gauges made of silicon and metals [25, 26]. To our best knowledge, no noise study of the proposed ink blend has been published so far. The few low-frequency noise measurements on non-commercial carbon resistors found in literature were mainly performed on either 10–35 μm thick screen-printed PTF on Al_2O_3 or FR-4 laminate for generic resistor application [12, 27, 28] or 0.06–2.3 μm thick spray-coatings intended for vapor sensing electronic nose [29–31]. A 2.5 μm-thick elastic resistor made of carbon-nanotube (CNT)-based ink screen-printed on Al_2O_3 is the closest case study found to our work in terms of material nature and device geometry. That work suggests CNT-based inks could be a serious alternative to carbon-black ones in elastic resistors thanks to their mechanical characteristics.

As screen-printing manufacturing, especially with composite inks, yields larger process variations and lower resolutions than typical microfabrication processes for thin films, it is tempting to consider the intrinsic noise as a minor concern compared to static device-to-device process-induced variations and this could explain why fewer noise analyses were carried out in this field. However, assessing the noise performance of such devices is becoming necessary as flexible electronics move towards high-sensitivity applications. Beyond the intrinsic thermal noise, previous works reported $1/f$ noise [3, 12, 32] and sometimes random telegraph noise [12]. Our work shows that the noise power in carbon-black-based inks screen-printed on Kapton substrate leads to a way lower signal-to-noise ratio (SNR) than for conventional silicon [25] or metal [26] gauges, but SNR over 100 dB is achieved with our devices. This is considered extremely promising for strain-sensing applications [33].

Moreover, we report power spectral density (PSD) analysis at lower bias currents, down to the μA range, than typically used in other studies (>300 μA [34] and most usually in the mA range for commercial gauge [26]), which is directly motivated by the interest in low-power consumption sensors. As will be highlighted, the contribution of the thermal (Johnson–Nyquist) noise, inherent to any dissipative devices, is not negligible compared to the $1/f$ noise contribution for the lowest bias currents and must be accounted for in a comprehensive noise power analysis. The influence of bias current, resistance value, and morphology will be discussed and different processes will be considered to offer a greater diversity of samples subject to inhomogeneities in the perspective of analyzing the quality of the printed resistors as a device.

2. Experimental Details

2.1. *Sample fabrication and morphological characterization*

The resistive bars are screen-printed using the custom blend of 60% Micromax$^{\mathrm{TM}}$ 7082M to 40% Micromax$^{\mathrm{TM}}$ 3571 weight ratio, through a 200-40 Koenen steel-mesh screen on a 127 μm Kapton HN substrate. The screen printer is an EKRA E2 semi-automatic machine and the fixed chosen printing parameters are as follows:

(i) A filling speed of 50 mm/s, for the filling squeegee to spread the ink layer on the screen.
(ii) A snap-off of 0.673 mm, kept low to reduce distortion.
(iii) A pressure on the printing squeegee of 1 bar.

Two parameters are varied to create the sets of resistors that are measured in this work: the printing speed, set at 10, 30 and 50 mm/s, and the drying time in ambient air before curing, respectively, of 26, 22 and 18 min. All samples have been cured in the same air oven at 150°C for 25 min. The contact pads are added on top of the printed resistive bar by thermal evaporation. An adhesion layer of 10 nm of Chromium is topped by the 2 μm Copper contact, as displayed in Fig. 1(a). The design of the six pads delimits five resistors of the same 0.3 mm width (W) with increasing length, measured for the three samples, as reported in Table 1.

The total length of each printed bar is 12 mm. Individual resistor thickness t and length L, measured with a white light interferometry (WLI) on a Polytec MSA500 setup, are given in Table 1. A difference of $\sim 2.3\,\mu$m, i.e., $\sim 49\%$, can be noted between minimum and maximum average thicknesses as a function of printing process, as can be expected [35, 36]. Topological WLI images of middle-sized resistances, named L3, representative of the three printed bars, can be found in Fig. 1.

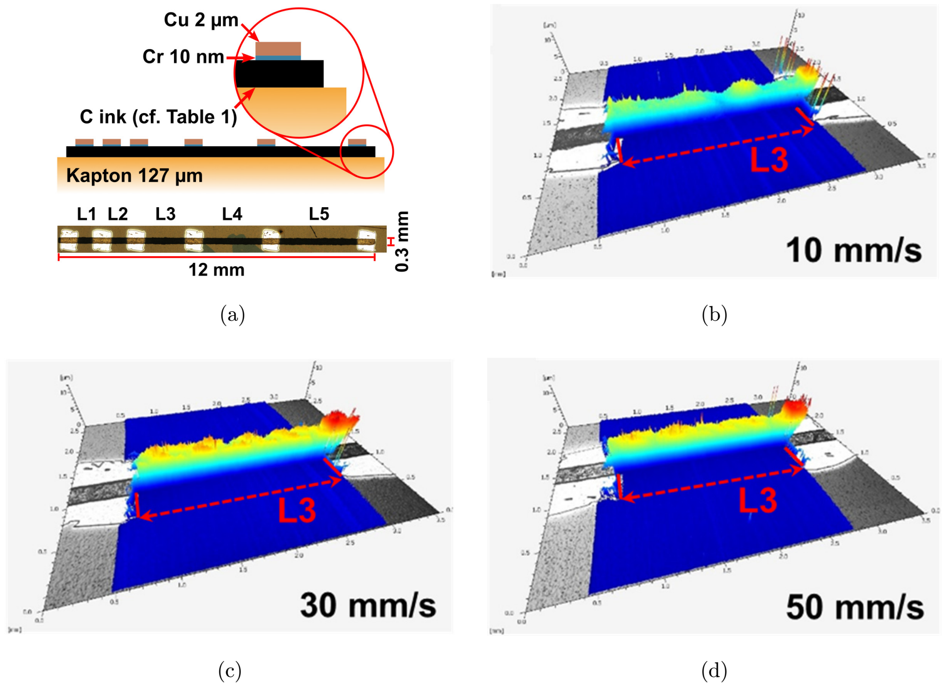

Fig. 1. Typical printed carbon ink line used in this work with variable contact pad edge-to-edge pitch from 0.83 mm to 4.2 mm with exact values related to position (cf. Table 1). (a) Micrograph and side-view schematic of the materials stack of the studied carbon line, (b)–(d) WLI 3D mapping of screen-printed L3 resistor at speeds 10, 30 and 50 mm/s, respectively.

Differences in morphology can be noted and linked to process variations, the main one being the height variation's locations, which are estimated by their standard deviation to range from 0.66 to 1.22 μm in Table 1. In this paper, samples are denoted by their printing speed to facilitate discussion, though the impact of other process variations, such as drying time, cannot be discarded at that stage.

Table 1. Lengths and mean thicknesses plus standard deviation values computed from Polytec MSA500 WLI data and resistance mean values and standard deviations over bias currents computed from MPI TS3000-SE300mm $I(V)$ measurements for the 15 studied resistors at three printing speeds.

		L1	L2	L3	L4	L5
10 mm/s	Length [mm]	0.85	0.89	2.17	3.15	4.11
	Thickness [μm]	4.71 ± 1.20	4.65 ± 0.74	4.80 ± 0.88	4.93 ± 0.98	4.81 ± 1.01
	Resistance [kΩ]	164 ± 0.7	153 ± 0.5	397 ± 5.1	581 ± 4.5	784 ± 7.3
30 mm/s	Length [mm]	0.93	0.90	2.16	3.14	4.04
	Thickness [μm]	6.86 ± 1.22	6.68 ± 1.01	6.64 ± 1.08	6.75 ± 1.03	6.74 ± 1.08
	Resistance [kΩ]	132 ± 0.1	125 ± 0.1	325 ± 3.7	465 ± 5.8	619 ± 4.1
50 mm/s	Length [mm]	0.88	0.83	2.13	3.14	4.20
	Thickness [μm]	6.84 ± 0.72	6.64 ± 0.77	6.59 ± 0.73	6.75 ± 0.70	6.95 ± 0.66
	Resistance [kΩ]	134 ± 0.2	128 ± 0.3	350 ± 5.3	508 ± 8.2	698 ± 6.1

2.2. *Electrical measurements*

The samples' resistances are individually measured using an MPI TS3000-SE300mm prober coupled with a Keysight B1500 analyzer and the results are given in Table 1. All the resistors were demonstrated to exhibit rigorous linear behavior (not shown here), without substantial standard deviations due to contact resistances or process irregularities (cf. Table 1). The mean resistance values range from 125 to 784 kΩ. Studied currents yield a voltage range between 62.5 mV for 125 kΩ at 0.5 μA, and 23.5 V for 785 kΩ at 30 μA, respectively, which represent appropriate values considering further strain gauge applications [1, 6].

The noise PSD measurements are carried out with an ALFNA Keysight noise analyzer as in [37]. In this setup, the resistors are biased at a constant voltage source Vr set by the equipment to reach a user-specified current target, Ir, according to the previously measured $I(V)$ characteristics. The equipment then measures current noise and we denote the obtained PSD $S_{ir}(f)$. Let us mention that previous works [26, 32, 34] studied the voltage noise PSD $S_{vr}(f)$, instead, under constant current. Without ambiguity for a linear resistance, these quantities relate according to Ohm's law (Thévenin from/to Norton noise model conversion):

$$S_{vr}(f) = R^2 S_{ir}(f) \tag{1}$$

Figure 2 depicts a typical current noise $S_{ir}(f)$ obtained from ALFNA measurements. For the seven Ir cases reported, the PSD reveals a typical $1/f$ noise behavior in the

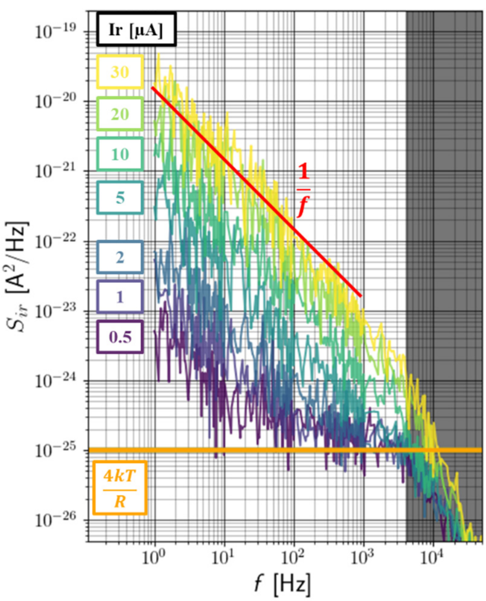

Fig. 2. Current noise PSD of the 153 kΩ carbon line resistor for seven bias currents. Color lines depict the $1/f$ trend and the thermal noise plateau. The dark region indicates the equipment roll-off. Illustrated case: resistance L2 printed at 10 mm/s (cf. Table 1).

low frequency range, on top of the thermal noise plateau ($4kT/R$) that is clearly dominant at higher frequency for the lowest biases. Such behavior is classical in thin-film resistive devices.

3. Noise Analysis Methodology

Processing of each measurement (one sample at a given bias current) consists of

(i) extracting the $1/f$ noise intensity,
(ii) verifying the thermal noise level $4kT/R$,
(iii) identifying and discarding any extrinsic environment- and setup-related noise sources.

Specifically, for each measurement, we fit an empirical $1/f$ noise model as in [37], whose general mathematical form is

$$S_{ir,\frac{1}{f}}(f) = \frac{K}{f^{\gamma}}. \tag{2}$$

The constant K indicates the fitted $1/f$ noise level at $f = 1\,\text{Hz}$. γ is usually close to unity but may typically vary from 0.8 to 1.2. Here, the K and γ of Eq. (2) are extracted for each measurement. The calculated total PSD is the sum of the independent $1/f$ noise and thermal noise components, i.e.,

$$S_{ir}(f) = S_{ir,\frac{1}{f}}(f) + S_{ir,th} = S_{ir,\frac{1}{f}}(f) + 4kT/R. \tag{3}$$

The noise power metric, denoted σ_{ir}^2 [37], is computed by integrating the total PSD Eq. (3) over a frequency bandwidth $[f_{min}, f_{max}]$ specified by the application:

$$\sigma_{ir}^2 = \int_{f_{\min}}^{f_{\max}} S_{ir}(f)df = \int_{f_{\min}}^{f_{\max}} S_{ir,\frac{1}{f}}(f)df + \frac{4kT}{R}(f_{\max} - f_{\min}) \tag{4}$$

In this work, $f_{\max} = 1\,\text{kHz}$ was used as a typical sensing bandwidth. The suitable $f_{\min}$ is related to the finite measurement time window T. A consistent formalism, as used for SPICE transient noise simulation [38], is to select $f_{\min} = 1/T$. T would be the typical duration of the sensor interrogation, e.g., 1 s. In the proposed framework, all the $1/f$ noise components of frequency smaller than 1 Hz are assimilated to quasi-static variations (akin to static process variability) and absorbed in the DC offset of the sensor that is usually calibrated and possibly corrected. The previous work [37], also based on Keysight LFNA, showed that the noise power provided by the integration of the PSD is very close to the empirical noise variance estimated from time series (not explicitly stored for the present work), provided that the same bandwidth is considered.

4. Results and Discussion

4.1. *Analysis of the 1/f noise*

The $1/f$ noise is suggested to be attributed to volume and surface traps inherent to the defects in such material and manufacturing process, as in [3, 12, 32]. To further investigate potential physical origins of the $1/f$ noise in our devices, we have computed the corresponding noise power $\sigma^2_{ir,\frac{1}{f}}$ provided with the equations described in Sec. 3.

In [32], the authors proposed a relationship between the spatially uncorrelated resistance fluctuations and the volume of the (possibly inhomogeneous) resistive sample. Only when the resistive bar is assimilated to an ideal parallelepiped, with homogeneous charge densities and constant electric field, the following simple relation is found [32]:

$$\frac{S_{vr}}{Vr^2} \sim \frac{1}{\text{Volume}}. \tag{5}$$

From Eq. (1), S_{vr}/Vr^2 in fixed-current measurement corresponds to S_{ir}/Ir^2 in the constant-voltage configuration adopted in this work. Considering Eq. (1), integrating Eq. (5) over the selected frequency bandwidth and remembering that $\text{Volume} = W \bullet t \bullet L$, the suggested trend to be investigated takes the form:

$$\frac{\sigma^2_{ir,\frac{1}{f}}}{Ir^2} \sim \frac{1}{L}. \tag{6}$$

Let us emphasize that, while Eqs. (5) and (6) are useful for assessing the consequences of material inhomogeneity on the noise behavior; we do not attempt in this work to thoroughly discuss the physical origin of the $1/f$ noise in carbon resistors. Vandamme's work [39] derived formulas similar to Eq. (5), however, more explicitly regarding the proportionality constant from a current crowding combined with a Hooge mobility fluctuation model. This approach is consistent with known $1/f$ noise model in commercial carbon resistors which originates from conductivity variations leading to uneven current flowing through the resistor [24]. Microarcs or microplasma discharges between carbon grains create sporadic current bursts, giving $1/f$ noise, so higher uniformity of resistor is the key to less noise. The validation of Vandamme's approach or the commercial carbon resistors model in the case of our samples is left for further work, since it would notably require varying the width of the resistive bars.

In order to evaluate the plausibility of Eq. (6), we have plotted in Fig. 3, $\sigma^2_{ir,\frac{1}{f}}/Ir^2$ as a function of individual bar resistor's normalized length (which is a reminiscence of [32], Fig. 4, here in terms of current fluctuations).

Almost all the resistances, printed at three different speeds and biased by two levels of current do follow the $1/L$ trend in Eq. (6), which indicates a certain electrostatic homogeneity within the samples. The bar printed at 10 mm/s measured at a current of 500 nA is believed to be an outlier whose non-typical behavior would require further investigation to relate it to the topological interferometry of Fig. 1(b).

If and only if the resistivity ρ and the transversal area (i.e., the sample thickness when the width is assumed finely controlled) of the carbon bar are believed constant (i.e., do not vary from one sample to another due to the process), the resistance equation for a homogeneous parallelepipedal bar $R = \rho L/S$ allows rewriting Eq. (6)

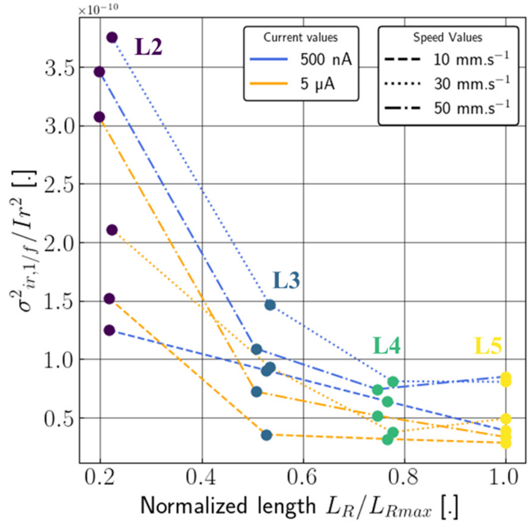

Fig. 3. $\sigma^2_{ir,\frac{1}{f}}/Ir^2$ versus normalized length for the three printing speed cases at two bias currents.

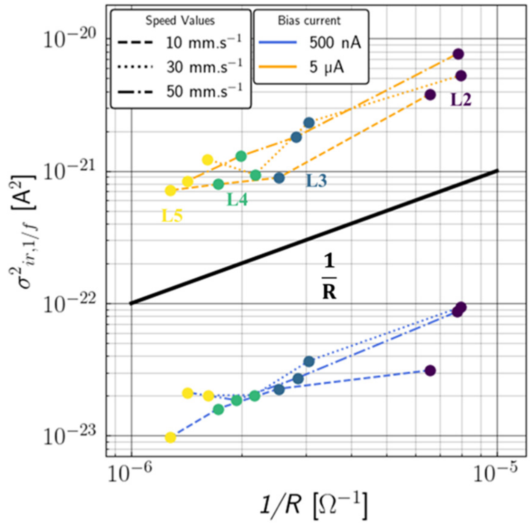

Fig. 4. $\sigma^2_{ir,\frac{1}{f}}$ versus the reciprocal of the resistance for two levels of currents on the three printed bars.

as

$$\frac{\sigma^2_{ir,\frac{1}{f}}}{Ir^2} \sim \frac{1}{R}, \tag{7}$$

now involving the sample resistance, which can be electrically characterized (to get rid of any uncertainty regarding the definition and measurement of the sample length) [40]. Resistivity values have been computed for each resistor from their mean resistance (over the seven bias currents) and mean geometrical parameters (computed with the WLI). The overall ink resistivity is found to be fairly constant with an average value of 0.305 Ω.m and a standard deviation of 0.021 Ω.m. In Fig. 4, we have thus plotted $\sigma^2_{ir,\frac{1}{f}}$ against individual resistances for both current levels. Most of our resistors closely verify Eq. (7) (trend shown in thick black line). As reviewed in [40], previous works explain deviations from that homogeneous behavior with percolation theory and model them empirically by adding an exponent η over R in Eq. (7).

From a design point of view, the observed trend, confirmed over the whole bias current range, highlights that a higher-resistance device is an asset for achieving an improved SNR, as studied in the next section.

4.2. *Combined contributions of thermal and 1/f noise and SNR*

Leveraging the definitions introduced in Sec. 3, Fig. 5 depicts the evolution of the integrated noise power with the bias current. The relative contributions of the thermal noise and the $1/f$ noise are shown.

The thermal noise power does not vary with the supply current, according to Johnson–Nyquist formula, and is a fundamental limit of detection for any resistance-

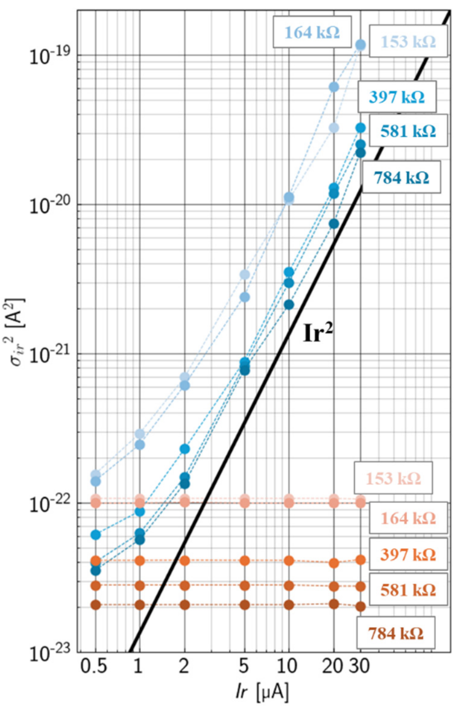

Fig. 5. Current noise power as a function of the target current for each individual measured resistor of the 10 mm/s printed bar and integrated in a practical frequency band of [1 Hz–1 kHz]: total $1/f$ and thermal noise (blue) and individual thermal noise component (orange). Illustrated case: carbon resistances printed at a speed of 10 mm/s.

based sensors. Nevertheless, we notice that $1/f$ noise significantly inflates the total noise power, and that this trend is, as expected, reinforced at larger currents. The increase of the $1/f$ noise intensity following $1/Ir^2$ can be explained by the spatially uncorrelated resistance fluctuation model Eq. (5) or Eq. (6), under the homogeneity assumption [32].

We end up this section with a perspective on the intrinsic quality of the printed resistors for sensing applications, by computing the SNR of our resistor measurements, according to its conventional definition, i.e., dividing the electrical power in the device by the noise power, which corresponds to [41] for a resistor biased at constant voltage:

$$\mathrm{SNR} = \frac{Ir^2}{\sigma_{ir}^2} \tag{8}$$

We point out an enhancement from 90 to 107 dB when increasing the current, as presented in Figs. 6(a) and 6(b), consistently with the conventional noise/power consumption trade-off. Figure 6(a) depicts the proportional SNR trend with resistance value. Increase of SNR with resistance confirms the potential of higher-resistance devices for low-cost, flexible and noise-robust strain sensors. This result is coherent with a decrease of $1/f$ and thermal contributions to total noise power with the increase of resistance observed in Figs. 4 and 5 of this section. From a low-power design point of view, it is important to note that the thermal noise plateau limits the reduction of the total noise power with $1/Ir^2$ for the lowest current range (Fig. 5). Low-power operation is then tied to degraded SNR, a noticeable trade-off for future sensor designs, as depicted in Fig. 6(b).

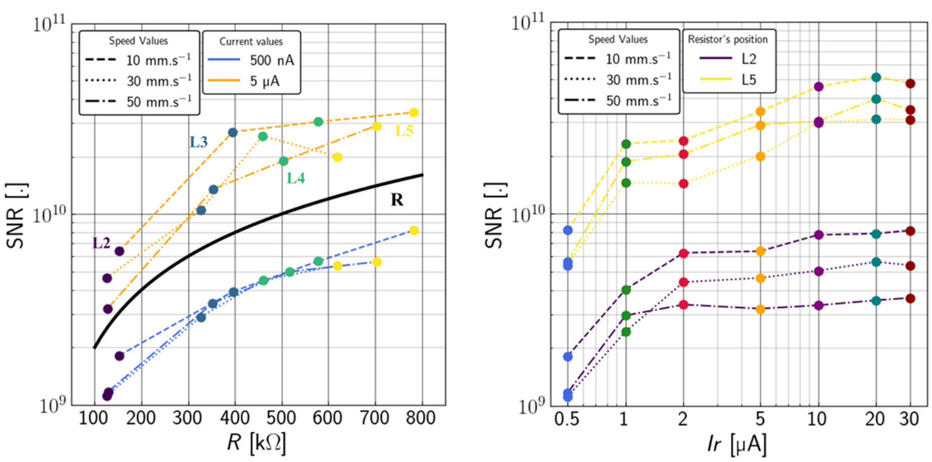

(a) (b)

Fig. 6. (a) SNR versus resistance for 500 nA and 5 μA and (b) SNR versus bias currents for short and long resistors for the three bars printed at different speeds.

Table 2. Comparison of the low-frequency noise performance with various strain gauges from the literature. SNR values marked with * have been computed from papers data.

Reference	Gauge material	$R[k\Omega]$	Bias current $I[\mu\,A]$	SNR range [.]	RI^2 [μ W]	V [mm^3]
[26][a]	Metal (PTF)	1	5 000	10^{15}–10^{16}*	$2.5.10^4$	$2.7.10^1$
[25][a]	Polysilicon	5.8–7.5	480	1–2.10^{13}*	1–2.10^3	1.10^{-6}
[34][a,b]	CNT-based PTFR	3.82	393–2 360	9.10^{10}–1.10^{11}*	6.10^2–2.10^4	4.10^{-2}
This work	Carbon-black-based PTFR	125–784	0.5–30	1.10^9–5.10^{10}	3.10^{-2}–7.10^2	1-9.10^{-3}

Notes: [a]S_{vr} are determined graphically at 1 Hz. [b]Values in $V/\sqrt{\text{Hz}}$ are converted into V^2/Hz.

4.3. *Benchmark and discussion*

We conclude this analysis by comparing the achieved SNR of our samples with previously published performance of conventional materials intended for gauge applications (notably commercial metallic resistors, polysilicon gauge) and CNT-based screen-printed resistor. The benchmark is summarized in Table 2. Values for the devices from the literature were computed following the same methodology applied to our experimental data, i.e., S_{vr} is converted to S_{ir} (1) knowing resistor values, integration is then performed in the same frequency bandwidth with Eq. (4) to finally compute the SNR with Eq. (8).

As could be anticipated from fabrication process considerations (i.e., related to the control of induced electrical defects), the commercial gauges made of metal and those microfabricated using silicon technology outperform the printed polymer material-based implementations such as ours. Our sensors exhibit a reduced SNR compared to the CNT of [34], but their bias currents and hence power consumption lie orders of magnitude below the other works. This is an advantageous asset towards an SNR versus energy trade-off. Table 2 further suggests the volume dependence of the SNR according to Eq. (5), which highlights another trade-off between size and precision. Overall, our lower power elastoresistors achieve an SNR as large as 100 dB when relying on larger resistance values, still representing a very good precision in actual sensing applications.

5. Conclusion

Screen-printed carbon resistors are promising strain sensor candidates but are prone to process-induced inhomogeneities. In comparison to mature conventional metal or semiconductor strain gauges, for which noise analyses are extensively documented, microfabricated sensors produced from a screen-printing process suffer from a lack of noise characterizations. This work fills this gap, presenting an extensive PSD analysis of carbon ink-based resistors with five lengths and three printing processes, analyzed over an applicative current range from 0.5 to 30 μA. Computed total noise power on a typical sensing frequency range shows that the expected SNR is proportional to resistance value and bias current, while process parameter variations influence remains small. This work shows that noise in the proposed printed carbon-black resistors is far from the performance of commercial equivalents. However, the high SNR ranging from 90 to 107 dB still qualifies these devices as good candidates for sensing applications with interesting potential trade-offs towards smaller size, higher resistance values and much lower power consumption.

Acknowledgments

This work was partially funded by the Wallonia Region through the CAPFLEX Win2Wal Project. The other part of the funding came from the FWB and the FRS-FNRS through the "chargé de recherche" grant supporting Van Brandt.

The authors wish to thank the CRM Group, Liège, Belgium, for access to the screen-printer and air oven, and for providing the screen and inks. Authors also wish to thank Winfab, UCLouvain, for the access to the facilities during sample fabrication, as well as the WELCOME technological platform for the access to the characterization equipment.

ORCID

Quentin Eynaud https://orcid.org/0009-0009-1871-9455
Eléonore Masarweh https://orcid.org/0000-0003-4025-565X
Valeriya Kilchytska https://orcid.org/0000-0002-8540-3313
Nicolas Marchal https://orcid.org/0000-0001-8150-7214
Denis Flandre https://orcid.org/0000-0001-5298-5196
Léopold Van Brandt https://orcid.org/0000-0003-4361-6537

References

[1] N. Anderson, N. Szorc, V. Gunasekaran, S. Joshi and G. Jursich, Highly sensitive screen printed strain sensors on flexible substrates via ink composition optimization, *Sens. Actuators A Phys.* **290** (2019) 1–7, doi: 10.1016/j.sna.2019.02.028.

[2] C. Yuan, A. Tony, R. Yin, K. Wang and W. Zhang, Tactile and thermal sensors built from carbon–polymer nanocomposites — a critical review, *Sensors (Switzerland)* **21**(4) (2021) 1–26, doi: 10.3390/s21041234.

[3] K. I. Arshak, L. M. Cavanagh and C. Cunniffe, Excess noise in a drop-coated poly(vinyl butyral)\carbon black nanocomposite gas sensitive resistor, *Thin Solid Films* **495**(1–2) (2006) 97–103, doi: 10.1016/j.tsf.2005.08.277.

[4] T. A. Khan, S. Nauman, Z. Asfar, M. A. Nasir and Z. M. Khan, Screen-printed nanocomposite sensors for online in situ structural health monitoring, *J. Thermoplast. Compos. Mater.* **33**(2) (2020) 236–253, doi: 10.1177/0892705718805131.

[5] J. M. Hale, Piezoelectric paint: Thick-film sensors for structural monitoring of shock and vibration, **1** (2004) 1–6, doi:10.1115/ESDA2004-58352.

[6] Y. Zhang, N. Anderson, S. Bland, S. Nutt, G. Jursich and S. Joshi, All-printed strain sensors: Building blocks of the aircraft structural health monitoring system, *Sens. Actuators A Phys.* **253** (2017) 165–172, doi: 10.1016/j.sna.2016.10.007.

[7] N. Graddage, H. Ding, C. Py, J. Lee and Y. Tao, Manufacturability of a printed resistance-based multiplexing scheme for smart drug packaging, *IEEE Trans. Compon., Packag., Manuf. Technol.* **6**(3) (2016) 335–345, doi: 10.1109/TCPMT.2016.2516401.

[8] E. Bihar, T. Roberts, M. Saadaoui, T. Hervé, J. B. De Graaf and G. G. Malliaras, Inkjet-printed PEDOT:PSS electrodes on paper for electrocardiography, *Adv. Healthc. Mater.* **6**(6) 1601167 (2017), doi: 10.1002/adhm.201601167.
[9] F. P. Wieringa, G. T. Van Heck, P. Rensing, M. M. Koetse, S. S. Kalisingh and H. Schoo, Systems in foil — Opening new perspectives in medical technology, *IFMBE Proc.* **22** (2008) 2292–2295, doi: 10.1007/978-3-540-89208-3_550.
[10] S. Park *et al.*, Fully screen-printed PI/PEG blends enabled patternable electrodes for scalable manufacturing of skin-conformal, stretchable, wearable electronics, *ACS Appl. Mater. Interfaces* **15**(1) (2023) 2092–2103, doi: 10.1021/acsami.2c17653.
[11] C. A. Gutierrez and E. Meng, Low-cost carbon thick-film strain sensors for implantable applications, *J. Micromech. Microeng.* **20**(9) (2010) 095028, doi: 10.1088/0960-1317/20/9/095028.
[12] A. W. Stadler, A. Kolek, K. Mleczko, Z. Zawišlak, A. Dziedzic and W. Stęplewski, Noise sources in polymer thick-film resistors, *Solder. Surf. Mt. Technol.* **27**(3), (2015) 115–119, doi: 10.1108/SSMT-04-2015-0014.
[13] X. Zhang, T. Ge and J. S. Chang, Fully-additive printed electronics: Transistor model, process variation and fundamental circuit designs, *Org. Electron.* **26** (2015) 371–379, doi: 10.1016/j.orgel.2015.07.058.
[14] B. Rambabu and Y. S. Rao, Universal trimming of polymer thick film resistors, *Microelectron. Int.* **32**(2) (2015) 45–51, doi: 10.1108/MI-09-2014-0038.
[15] J. Chang, X. Zhang, T. Ge and J. Zhou, Fully printed electronics on flexible substrates: High gain amplifiers and DAC, *Org. Electron.* **15**(3) (2014) 701–710, doi: 10.1016/j.orgel.2013.12.027.
[16] T. Ge, J. S. Chang, T. Lin, Z. Lei and L. G. Soon, Fully-Additive printed electronics on flexible substrates: A fully-additive RFID tag, in *Midwest Symp. Circuits and Systems* (IEEE, 2014), pp. 825–828, doi: 10.1109/MWSCAS.2014.6908542.
[17] M. S. Mills, Additive manufacturing of RF absorbers, thesis, Faculty of the University of Delaware (2016).
[18] N. Jess and B. Syrett, A new hybrid-polymer optically tunable dielectric and its measurement using a variation on the split-post dielectrc resonator, *Microw. Opt. Technol. Lett.* **55** (2013) 1304–1305, doi: 10.1002/mop.27545.
[19] S. P. M. and L. R. J. M. Gonzalez, N. Delhote and D. Baillargeat, Optically tunable filter based on meshed CDS-polymer MIM capacitor, *Microw. Opt.* **58** (2016) 1926–1929, doi: 10.1002/mop.29939.
[20] T. Morolari, L. Roy and B. Syrett, Microwave characterization of optically sensitive polymer and application to a tunable antenna, in *2010 14th Int. Symp. Antenna Technology and Applied Electromagnetcis and the American Electromagnettics Conf. ANTEM/AMEREM 2010* (IEEE, 2010), pp. 1–4, doi: 10.1109/ANTEM.2010.5552531.
[21] E. Masarweh, M. Arseenko, P. Guaino and D. Flandre, Membrane-based mechanical characterization of screen-printed inks: Deflection analysis of ink layers on polyimide membranes, *Appl. Res.* **3**(4) (2024) 1–8, doi: 10.1002/appl.202300113.
[22] S. Suh, R. Persons, D. Hargrove and G. Berube, Solderable polymer thick-film conductors for low temperature substrates, *Int. Symp. Microelectron.* **2018**(1) (2018) 000310–000316, doi: 10.4071/2380-4505-2018.1.000310.
[23] G. M. Berube, Thick-film — a mature technology at the cutting edge of advances in the electronics industry, *Adv. Microelectron.* **2022**(IMAPS Symposium) (2022) 487–492, doi: 10.4071/001c.74534.
[24] C. D. Motchenbacher and J. A. Connelly, *Low-Noise Electronic Design*, Vol. 19, No. 21 (John Wiley & Sons, 1973), doi: 10.1049/ep.1973.0635.

[25] L. Michelutti, N. Mathieu, A. Chovet and A. Galerie, Influence of chemical corrosion on resistivity and 1/fnoise of polysilicon gauges, *Microelectron. Reliab.* **40**(1) (2000) 179–183, doi: 10.1016/s0026-2714(99)00215-2.

[26] D. Walter, A. Bülau and A. Zimmermann, Review on excess noise measurements of resistors, *Sensors* **23**(3) (2023) 1107, doi: 10.3390/s23031107.

[27] A. Dziedzic and A. Kolek, 1/fnoise in polymer thick-film resistors, *J. Phys. D: Appl. Phys.* **2091** (1998).

[28] K. Mleczko, P. Ptak, Z. Zawiślak, M. Słoma, M. Jakubowska and A. Kolek, Noise properties of graphene-polymer thick-film resistors, *Metrol. Meas. Syst.* **24**(4) (2017) 589–594, doi: 10.1515/mms-2017-0051.

[29] B. Matthews, J. Li, S. Sunshine, L. Lerner and J. W. Judy, Effects of electrode configuration on polymer carbon-black composite chemical vapor sensor performance, *IEEE Sens. J.* **2**(3) (2002) 160–167, doi: 10.1109/JSEN.2002.800284.

[30] S. M. Briglin, M. S. Freund, P. Tokumaru and N. S. Lewis, Exploitation of spatiotemporal information and geometric optimization of signal/noise performance using arrays of carbon black-polymer composite vapor detectors, *Sens. Actuators B Chem.* **82**(1) (2002) 54–74, doi: 10.1016/S0925-4005(01)00991-1.

[31] C. Falconi *et al.*, $1/f$ noise and its unusual high-frequency deactivation at high biasing currents in carbon black polymers with residual $1/f\Gamma(\Gamma = 2.2)$ noise and a preliminary estimation of the average trap energy, *Sens. Actuators B Chem.* **174** (2012) 577–585, doi: 10.1016/j.snb.2012.07.095.

[32] A. Kolek and A. Dziedzic, Low-frequency noise of polymer thick-film resistors: analysis of volume and contact effects, in *2000 22nd Int. Conf. Microelectronics, MIEL 2000 — Proc.*, Vol. 2 (IEEE, 1999), pp. 531–534, doi: 10.1109/icmel.2000.838747.

[33] C. Tang *et al.*, Ultrasensitive textile strain sensors redefine wearable silent speech interfaces with high machine learning efficiency, *npj Flex. Electron.* **8**(1) (2024) 1–11, doi: 10.1038/s41528-024-00315-1.

[34] M. Sloma *et al.*, Investigations on printed elastic resistors containing carbon nanotubes, *J. Mater. Sci. Mater. Electron.* **22**(9) (2011) 1321–1329, doi: 10.1007/s10854-011-0307-z.

[35] N. Kapur, S. J. Abbott, E. D. Dolden and P. H. Gaskell, Predicting the behavior of screen printing, *IEEE Trans. Compon., Packag., Manuf. Technol.* **3**(3) (2013) 508–515, doi: 10.1109/TCPMT.2012.2228743.

[36] D. E. Riemer, The theoretical fundamentals of the screen printing process, *Microelectron. Int.* **6**(1) (1989) 8–17, doi: 10.1108/eb044350.

[37] L. Van Brandt, B. K. Esfeh, V. Kilchytska and D. Flandre, Robust methodology for low-frequency noise power analyses in advanced MOS transistors, in *2019 Jt. Int. EUROSOI Work. Int. Conf. Ultimate Integration on Silicon, EuroSOI-ULIS 2019*, No. 2 (IEEE, 2019), doi: 10.1109/EUROSOI-ULIS45800.2019.9041859.

[38] L. Van Brandt *et al.*, Modeling and predicting noise-induced failure rates in ultra-low-voltage SRAM bitcells affected by process variations, *IEEE Trans. Circuits Syst. I, Regul. Pap.* **72**(3) (2025) 989–1002, doi: 10.1109/TCSI.2024.3525387.

[39] E. P. Vandamme and L. K. J. Vandamme, Current crowding and its effect on 1/fnoise and third harmonic distortion — a case study for quality assessment of resistors, *Microelectron. Reliab.* **40**(11) (2000) 1847–1853, doi: 10.1016/s0026-2714(00)00091-3.

[40] A. Dziedzic, Carbon/polyesterimide thick-film resistive composites — experimental characterization and theoretical analysis of physicochemical, electrical and stability properties, *Microelectron. Reliab.* **47**(2–3) (2007) 354–362, doi: 10.1016/j.microrel.2006.02.016.

[41] R. P. Troisi, Ultra-low-power interface circuits for gas sensors with a high resistance range, Doctoral dissertation, UCL — Université Catholique de Louvain (2025).